Impact damage on a thin glass plate with polycarbonate backing

Authors: Wenke Hu[1], Jian Yu[2], Chian-Fong Yen[2], and Florin Bobaru[1*]

1. Department of Mechanical and Materials Engineering, University of Nebraska-Lincoln, Lincoln, NE 68588, United States

2. U.S. Army Research Laboratory, Aberdeen Proving Grounds, MD 21005, United States

* Corresponding author: fbobaru2@unl.edu

Abstract We present experimental and computational results for the impact of a spherical projectile on a thin glass plate with a thin polycarbonate backing plate restrained in a metal frame. We analyze the dependence of the damage patterns in the glass plate on the increasing impact velocities, from 61m/s to 200m/s. Experimental results are compared with those from peridynamic simulations of a simplified model. The main fracture patterns observed experimentally are captured by the peridynamic model for each of the three projectile velocities tested. More accurate implementation of the actual boundary conditions present in the experiments will likely improve modeling of brittle damage from impact on a multi-layered system further. The peridynamic computational model allows for a depiction of the early stages of the complex damage evolution in the glass layer.

Keywords: glass; multi-layer; brittle fracture; impact; peridynamics; fragmentation; dynamic fracture.

1. Introduction

Due to their low cost of manufacturing, light weight, and high performance, glass laminates are widely used in skylight glazing and in windshields for automobile, train, and military vehicle. In order to design and improve glass laminates for protective applications, it is important to be able to predict the damage and fracture behavior of glass plates under impact.

Experiments have been conducted in the past (see [1-8]) to analyze the behavior of a single glass plate or glass laminates subject to low or high impact velocity. Knight et al. [1] found that the Hertzian cone angle decreases with increasing impact velocity for a glass block under small steel

spheres impact. Ball and Mckenzie [2] performed a series of impact tests on circular float glass plates with thicknesses between 3 mm and 12 mm with various impact speed (10 - 50m/s). They identified a number of failure mechanisms in the plates and constructed a fracture map which incorporates the effect of plate thickness and impact velocity. Important contributions to experimental analysis of damage in glass from impact and understanding the mechanisms of brittle failure from solid particle impact have been made over several decades by the group at Cavendish laboratory at University of Cambridge (see [3]). For example, Field ([4], [5]) and Field and Sun [6] studied the impact of small steel spheres on a range of glasses and ceramics. They give tables of the threshold velocities at which different damage mechanisms operate. For instance, in glasses, single cone cracks can be formed up to 40m/s, while at higher impact speeds, stress wave damage rather than a 'quasistatic' response is obtained. Their research ([4], [5], [6]) also identified important differences in the response depending on whether the ratio of the hardness of the projectile to the target was greater or less than 1.The thickness of the glass plate in relation to the impact velocity, and the angle of impact are also important factors affecting the progression of damage in glass (see [1], [7]). The picture of damage progression is further complicated in multi-layered systems due to the stress wave reflections from the various interfaces. Multi-layer glass laminates subject to high velocity impact display very complex damage pattern by dynamic brittle fracture through the layers. Bless et al. [8] studied the morphology of damage from high velocity impact (1120m/s) onto a seven-layer glass laminate with a polycarbonate backing.

Developing models that can correctly capture all the observed features of dynamic fracture and fragmentation from impact on glass plates and laminates has been extremely challenging. A number of numerical studies based on the finite element method (FEM) or molecular dynamics [9-12] have been performed to compute the response of glass plates and laminates under impact loading. In the work of Timmel et al ([9]), glass laminates with a PVB-interlayer under low impact velocity are modeled using LS-DYNA shell elements and a failure criterion based on the principal strain reaching a critical value. Element deletion is used as the elements fail. The fracture behavior is highly mesh dependent and certain meshes lead to unrealistic results. Finite elements with element deletion method (sometimes called "vanishing element technique" or "element erosion method") are also used in [10], with a stress-based continuum damage model for describing the constitutive behavior of glass. The contribution of different cracking systems

is explicitly taken into account in this work. The authors of [10] study the initiation and propagation of the ring/cone crack in a glass plate under impact based on this model. They obtained multi-ring cracks when using a higher critical stress value in contrast with extensive crushing and ejected debris when the critical stress value used was lower. Since a 2D axisymmetric model is used in [10], only a limited set of cracks are obtained: for instance, radial cracks cannot be simulated with this approach.

Motivated by experimental observation of glass failure, the authors of reference [11] proposed a model based on the idea that a critical energy value must be reached over a *finite region* before the glass can fail, independent of the calculated stress. This is a nonlocal damage model. A finite element model using shell elements implements this nonlocal criterion for a compound glass-PVB-glass system and uses element deletion once failure is determined to occur. While the nonlocal damage model improves the simulation results compared with local damage models, the obtained damage morphology differs in significant ways with the experimentally observed one.

At the other end of the spectrum in terms of modeling failure of glass, atomistic models have been used recently (see e.g. [12]) to study the fracture of silica glass from hypervelocity impact. The authors of [12] report cracks initiate and propagate from the bottom to the top of the 24 nano-meter thick glass sheet. Molecular dynamics (MD) models, however, cannot be used to model macro-scale structures, while multiscale models coupling MD with FEM models, for example, need to take into account the well known fact (see e.g. [13]) that stress waves that propagate and reflect from the boundaries strongly affect the evolution of fracture in a brittle system. Therefore, to accurately capture the evolution of damage in brittle systems, the entire structure needs to be considered in the simulations and the dynamics of the stress waves, in the presence of evolving damage and failure fronts, needs to be solved for correctly.

In the present paper, we report on results from experimental and numerical studies using peridynamics on impact on a two-layer square laminate composed of a thin (33 mm) glass plate and a thin (30 mm) polycarbonate backing plate with sides of about 10 cm. The two-layer system is placed in a metallic frame and impacted with a spherical projectile at speeds ranging from 61 m/s to 200 m/s. We will refer to this glass-polycarbonate system as the G-PC system. The numerical studies conducted with peridynamics, using the code EMU (see [14]) with some modifications of the spatial integration detailed in [15] are performed for a model which only

approximates the presence of the actual aluminum frame used in the experiments. The recently introduced nonlocal continuum model, peridynamics [16], is well suited for solving dynamic fracture problems (see e.g. [17], [18], [19], [20],[21], [22]). In order to overcome mathematical inconsistencies in the classical continuum mechanics models of problems in which cracks are initiated *and evolve* in time, peridynamics uses an integral of forces (per volume-squared) over a nonlocal region (called horizon) around a point to replace the divergence of the stress tensor in the equations of motion. The method has been shown to correctly predict phenomena in dynamic fracture in brittle materials and composite materials, including crack branching and the crack propagation speed [16-20].The role of the "influence function" on the peridynamic results for impact damage on a glass cylinder from a spherical projectile has been studied in [23].

Here, we employ the simplest peridynamic constitutive model for a brittle material (linear micro-elasticity with brittle damage) and observe that we capture most of the damage morphology seen in the experiments, including the changes induced by the higher impact speed on the damage patterns. Furthermore, the trend for the projectile rebound speed compares favorably with the experimental results. The boundary conditions used in the simulations are for a more rigid setting than those present in the experiments; most of the differences between the computational results and the experimental observations can be attributed to the rigidity of the boundary conditions used here to approximate the holding metal frame employed in the experiments. The evolution of damage and its connection to the stress waves' propagation in the two-layer system is described in detail.

The paper is organized as follows: in Section 2, the experimental tests are described and the investigation of damage patterns dependence on the impact speeds is presented; in Section 3, we briefly review the basic formulation for peridynamics and the damage model used; in Section 4, we present the numerical results from the peridynamic model of the impact on the G-PC system and compare them with the experimental results. We also include a description of the early stages of damage evolution in the glass layer, based on the computational model results. Conclusions are given in Section 5.

2. Experiments of impact on the glass-polycarbonate system

2.1 Experimental setup

The two layer glass-polycarbonate (G-PC) system tested at the ARL lab consists of a square soda-lime glass plate with dimensions 10.16 cm × 10.16 cm × 0.33 cm, and a backing polycarbonate layer of 10.16 cm × 10.16 cm × 0.3 cm. An aluminum frame holds the G-PC plates together and has the same outer dimensions as the G-PC laminate, but has an opening of 5.08cm × 5.08cm (see Figure 1). The inside surface of the frame is lined with a 1mm thick rubber gasket. Tests were also performed without rubber gasket but no major differences are observed between these two conditions in terms of damage patterns. The frame, along with the G-PC system, is clamped on the edge to a target fixture for impact testing. A spherical projectile (440C stainless steel) with 0.556 cm diameter and 0.692 g mass is shot from a gas gun normal to the center of the glass plate at different velocities: 61, 100, and 200 m/s.

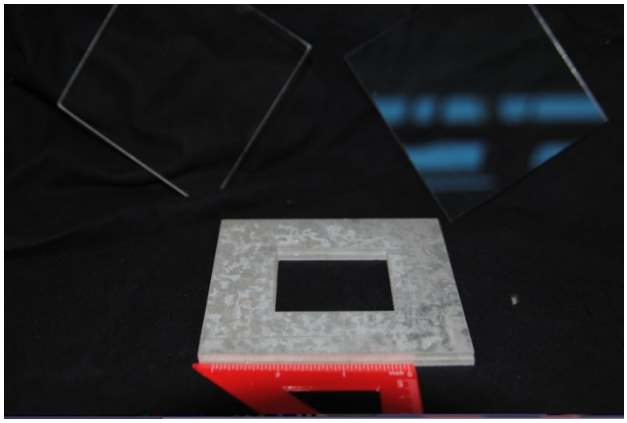

Figure 1. Experimental setup. The glass and polycarbonate plates are sandwiched between two metal frames and clamped together at the outer edge.

2.2 Experimental results and discussion

Figure 2 shows the post-mortem samples (glass plate only) impacted at three different velocities. The polycarbonate plate is not damaged at the lower two impact velocities and at 200 m/s only some minor plastic deformation is observed near the impact. The signature of the metal frame opening is visible from the cracks enclosed in the rectangular regions marked on the figures in each of the three impact speed cases. Note that clamping is not at the opening's edges but on the outer edges of the frame, thus some separation between the glass and PC layers, and the metal frame is possible and likely takes place during the impact. This possible separation explains the non-uniformity of the cracks in the frame opening area. Radial cracks emanating from the impact crater are observed in all cases, but with some differences in terms of the length and number of

these radial cracks, which depend on the impact velocity. Circumferential cracks or ripple cracks (see elliptical regions in Figure 2) become denser as the impact speeds increase. Some of the through-thickness cracks are not perpendicular to the plane of the plates, instead they are tilted, as they can be seen from the light reflections in the diamond regions. For impact speeds of 100 m/s and 200 m/s, some of the radial cracks split (or branch) as seen inside the circular regions. If these cracks form from the edges, however, then they are coalescing, instead of branching. These features seem to associate primarily with cracks that split the plate into four quadrants, which are called quadrant cracks in [8]. In the 100 m/s case, we also observe the formation of cracks that do not connect to the central region, thus they could grow from the boundaries, as seen in the triangular regions. These cracks are harder to distinguish in the 200 m/s case due to the severe fragmentation that had taken place. Corner cracks cutting the corners at 45 degrees (see square regions) from the impact velocity of 200 m/s at three of the four corners. These types of cracks are absent at impact speeds of 61m/s and 100m/s.

At the two low impact speeds (61 m/s and 100 m/s), no visible damage is observed in the polycarbonate plate, aside from some superficial surface scratches. At these impact speeds, the projectile rebounds from the target with speeds of about 3 m/s and 8 m/s, respectively. At a high impact speed of 200 m/s, plastic deformation near the impact site is observed in the polycarbonate plate but no cracks or penetration. At this impact speed the projectile rebounds from the G-PC system faster than the rebound from the two other two impact speeds, at about 33 m/s.

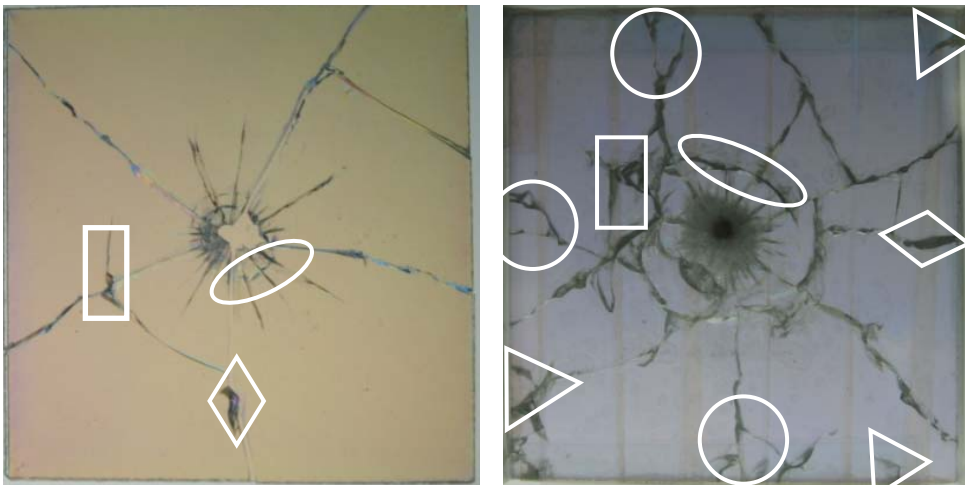

[61 m/s] [100m/s]

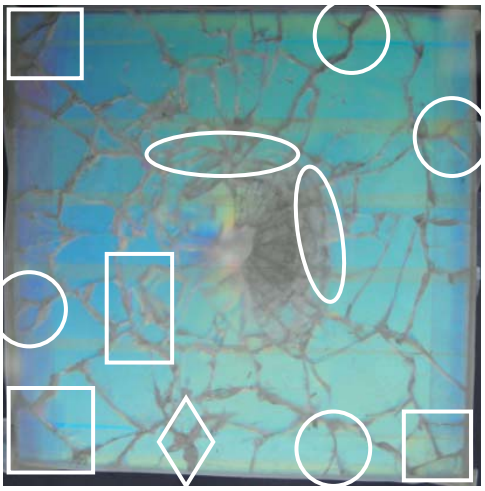

[200 m/s]

Figure 2. Experimental results: damage patterns in the glass layer under various impact speeds. The signature of the frame opening is indicated by rectangular regions, diamonds highlight through-thickness titled cracks, ellipses contain ripple cracks, circles surround splitting cracks, some boundary cracks are inside the triangles, and squares show corner cracks.

Some glass fragments around the impact crater were lost during the impact on the strike face. Tape was used to hold the pieces together after the tests. At the highest impact speed, the predominant damage pattern outside of the central region, where the fine and dense radial and circumferential cracks are formed, is fragments of glass that have some resemblance to intersecting radial and circumferential cracks. However, in this case, the “radial” and “circumferential” cracks are discontinuous and not well organized, the picture showing mostly irregular “islands” of unbroken glass. Cracks that split near the boundaries, or that coalesce if

they are actually starting from the boundaries, are observed as well on each of the four sides. A unique feature observed at the high impact speed and not seen at 61 or 100 m/s, is the presence of corner cracks.

3 Review of the peridynamic formulation

Introduced by Silling [16], the peridynamic theory is a non-local formulation that extends the classical continuum mechanics formulation. The term "peridynamics" comes from the Greek roots for "nearby" and "force" [16]. In peridynamics, every material point is connected to the other points inside a certain "horizon" region through peridynamic bonds. Instead of the stress divergence term in the classical equations of motion for a continuum, an integral of forces per volume-squared in the bonds at a point, over the current point horizon region is used. The peridynamic equations of motion are:

$$\rho\ddot{\mathbf{u}}(\mathbf{x},\mathrm{t}) = \int_H \mathbf{f}(\mathbf{u}(\mathbf{x},\mathrm{t}) - \mathbf{u}(\mathbf{x},\mathrm{t}), \hat{\mathbf{x}} - \mathbf{x})\mathrm{dV}_{\hat{\mathbf{x}}} + \mathbf{b}(\mathbf{x},t)$$

where **f** is the pairwise force function in the peridynamic bond that connects point $\hat{\mathrm{x}}$ to **x,** and **u** is the displacement vector field. ρ is the density and **b**(**x**, *t*) is the body force. The integral is defined over a region *H*, the compact supported domain of the pairwise force function around a point **x**, called the "horizon region". The region is taken here to be a sphere of radius δ. The peridynamic horizon may be viewed as an "effective" interaction distance or an "effective length-scale" of a continuum [21]. In principle, the exact size and shape of the horizon could be found from wave dispersion curves for a specific material under specific dynamic conditions (see [16], [24]).

Let $\boldsymbol{\xi} = \hat{\mathbf{x}} - \mathbf{x}$ be the relative position in the reference configuration and $\boldsymbol{\eta} = \hat{\mathbf{u}} - \mathbf{u}$ the relative displacement between two material points, **x** and $\hat{\mathbf{x}}$. From the definition of the horizon, we have

$$\|\boldsymbol{\xi}\| > \delta \Rightarrow \mathbf{f}(\boldsymbol{\eta},\boldsymbol{\xi}) = 0$$

A micro-elastic material is defined as one for which the pairwise force derives from a micropotential ω:

$$\mathbf{f}(\boldsymbol{\eta},\boldsymbol{\xi}) = \frac{\partial\,\omega(\boldsymbol{\eta},\boldsymbol{\xi})}{\partial\boldsymbol{\eta}}$$

The strain energy density at a given point is defined as:

$$\mathrm{W} = \frac{1}{2}\int_H \omega(\boldsymbol{\eta},\boldsymbol{\xi})\mathrm{dV}_{\xi}$$

The factor 1/2 factor is present because the elastic energy in a bond is shared by the two nodes connected by the bond. A *linear* micro-elastic potential, which leads to a linear relationship between the bond force and the relative elongation of the bond, is obtained if we take

$$\omega(\boldsymbol{\eta},\boldsymbol{\xi}) = \frac{c(\|\boldsymbol{\xi}\|)s^2\|\boldsymbol{\xi}\|}{2}$$

where s is the bond relative elongation

$$\mathrm{s} = \frac{\|\boldsymbol{\xi}+\boldsymbol{\eta}\| - \|\boldsymbol{\xi}\|}{\|\boldsymbol{\xi}\|}$$

The corresponding pairwise force becomes

$$\mathbf{f}(\boldsymbol{\eta},\boldsymbol{\xi}) = \frac{\partial\omega(\boldsymbol{\eta},\boldsymbol{\xi})}{\partial\boldsymbol{\eta}} = c(\|\boldsymbol{\xi}\|)s\frac{\partial\|\boldsymbol{\xi}+\boldsymbol{\eta}\|}{\partial\boldsymbol{\eta}}$$

The function $c(||\boldsymbol{\xi}||)$ is called the micromodulus function and represents the bond elastic stiffness. For isotropic materials, the micromodulus function version is computed by matching the peridynamic strain energy density to the classical strain energy density

$$W_{\text{classical}} = \frac{1}{2}\int_H \frac{c(\|\boldsymbol{\xi}\|)s^2\|\boldsymbol{\xi}\|}{2}dV_{\hat{\mathbf{x}}}$$

The value for the 3D constant micromodulus function is then derived as (see [25])

$$c = \frac{18k}{\pi\delta^4}$$

where k is the bulk modulus.

The damage model in peridynamics consists in breaking the peridynamic bonds connecting any two nodes when the relative change in distance between them exceeds a certain prescribed value s_0 [16]. This critical relative elongation parameter s_0 is obtained by equating the work, per unit fractured area, required to break all the bonds across a surface, to the fracture energy required for complete separation along the surface (see [25])

$$\mathrm{G}_0 = \int_0^{\delta}\int_0^{2\pi}\int_{\mathrm{z}}^{\delta}\int_0^{\cos^{-1}(\mathrm{z}/\|\boldsymbol{\xi}\|)}[c(\|\boldsymbol{\xi}\|)s_0^2\|\boldsymbol{\xi}\|/2]\|\boldsymbol{\xi}\|^2\sin\phi\,\mathrm{d}\phi\,\mathrm{d}\xi\,\mathrm{d}\theta\,\mathrm{dz}$$

For the constant micro-modulus given above, the critical relative elongation is obtained as

$$s_0 = \sqrt{\frac{10G_0}{\pi c \delta^5}}$$

We impose the same s_0 over the entire region, which results in an effectively slightly weaker material in the regions near the boundary or where damage already happened, since the integration region is reduced compared to a location in the undamaged bulk. This is similar to the skin effect discussed in [15]. A damage-dependent s_0 can be introduced in order to reduce the effectively weaker bond strength near the boundary or in damaged regions (see [25], [18]). Especially in impact problems where many new boundaries are formed as a result of a multitude of newly created fracture surfaces, a constant critical relative elongation may result in the over prediction of the number of fragments formed. In this paper we choose to "strengthen" the material in damaged regions by allowing s_0 to depend monotonically on the amount of damage at that particular node. One could attempt an exact evaluation of the damage-dependent (variable) s_0. However, here we resort to a simpler way, namely an approximation proposed in [14] which is described by the following formula

$$s = \begin{cases} s_0 \times \min\left[\gamma, 1 + \beta \times \dfrac{D-\alpha}{1-D}\right], & \text{if } D > \alpha \\ s_0, & \text{otherwise} \end{cases}$$

where the damage index D is defined as the ratio of the number of broken bonds to the number of initially bonds. s_0 and s are the initially given critical relative elongation and the computed critical relative elongation, respectively. In the simulations that follow, we use the values $\alpha = 0.35$, $\beta = 1$, and $\gamma = 2$. More details can be found in [18].

A validation of the peridynamic micro-elastic model against a finite element model has been performed in [22], where a comparison of the elastic bending deformation between the nonlocal solution for the problem of elastic impact, in which no damage is allowed to initiate, with the horizon size of about 2.7 mm and a grid spacing less than 1 mm, and a dynamic (explicit) finite element solution obtained by using Abaqus. The results for the bending deformation in the problem of elastic impact of a spherical rigid projectile onto a two-layer glass backed by a polycarbonate layer given by a converged finite element solution with solid elements and the peridynamic model that uses a grid of comparable size were shown to match very well. The time-evolution for the projectile speed also matches well between the two different models (see [22]).

For the model with damage, the comparison of the peridynamic results will be made with the experimental results discussed in Section 2.

4. Peridynamic results for impact on the thin-plate glass-polycarbonate system

4.1 Problem setup

The peridynamic model for the two layer G-PC system uses the geometry and boundary conditions shown in Figure 3. The geometrical dimensions are the same as in the experiments, but the boundary conditions are slightly differed from those present in the experiments. For example, in the experiment, two metal frames with clamps are used in order to hold the specimen. Since a model that includes the metal plate, the clamps, and the holding fixture would lead to a much larger computational simulation, we choose here to approximate the actual boundary conditions with following: zero out-of-plane displacements (z-direction in Figure 3) for the nodes on the top face of the glass plate and bottom face of the polycarbonate layer, over the frame region (see Figure 4).

In the experimental samples, there is no adhesive layer between the glass and the polycarbonate. In the computational model, we "disconnect" all the peridynamic bonds between the two different material regions (glass and polycarbonate) and use simple non-penetrating contact conditions to describe contact conditions.

The material properties used in the model for soda-lime glass are: density $\rho = 2440$ kg/m^3, Young's modulus $E = 72$ GPa, facture energy $G_0 = 8$ J/m^2. In the experimental results, no damage is observed in the polycarbonate layer, except for the highest impact speed where some plastic deformation is visible. As a consequence, in the peridynamic simulations of the polycarbonate layer we prescribe "no-fail" conditions, by using a sufficiently large critical relative elongation that is never met during the simulation. The material properties for the polycarbonate layer are: density $\rho = 1200$ kg/m^3, Young's modulus $E = 2$ GPa. In bond-based peridynamics, the version used in this paper, the Poisson's ratio is fixed and equals 0.25 in 3D (close to the soda-lime glass Poisson ratio of 0.22), and 1/3 in 2D, since the assumption is that material points interact only through a pair-potential. The Poisson ratio limitation is removed in the state-based formulation of peridynamics (see [26]), however, here we use the bond-based for simplicity. We note that, in dynamic fracture problems of the type considered in this work, the

Poisson ratio value does not have a significant influence on the crack propagation speed or the shape of the crack path (see[17], [26]).

In the simulations, we use a spherical *rigid* projectile of the same dimensions and mass as the steel projectile used in the experiments and described in Section 2. The use of a deformable projectile is left for the future.

We perform the simulations using the same impact speeds as those used in the experiments. Based on a convergence study performed in [27], we select to use a horizon size $\delta = 1$ mm and $m = \delta / \Delta x = 4$, where Δx is the grid spacing used for the discretization of the domain integral in the peridynamics equations of motion. The selection is based on the damage patterns results and the projectile speed after perforation of a single glass plate (see [27]). Discussions about the dependence or independence of the crack propagation speed on the horizon size are given in [21]and [22]. The 3D discrete model has a total of over 6 million nodes (about 20 million degrees of freedom). The total simulation time is 77 μs with a time step size of about 27.5 ns. We use 100 processors on 2.2GHz/64 bit Opteron Linux cluster with 70Gb memory.

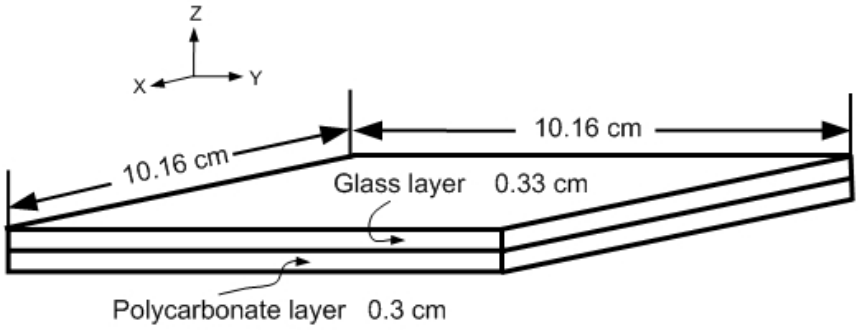

Figure 3. Dimensions for the two-layered glass-polycarbonate system.

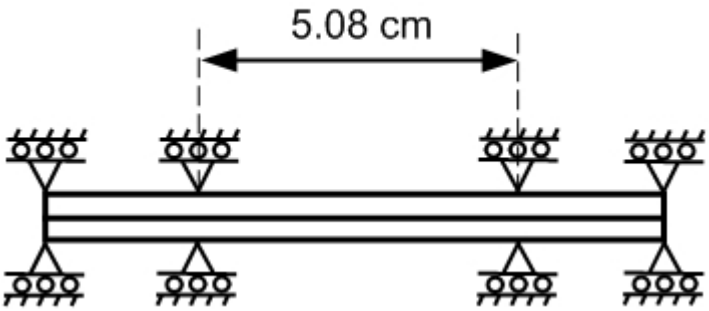

Figure 4. Through-thickness view (along the x-z plane passing through the center of the plate) of the boundary conditions for the glass-polycarbonate system.

4.2 Damage maps for different impact velocity: results and discussions

The peridynamic results for the damage of the glass plate are presented in terms of nodal damage index maps. The damage index d at a node is defined as:

$$d = \frac{n_{\text{broken}}}{n}$$

where n_{broken} and n are the number of broken bonds and the number of initial bonds at a node, respectively. The damage index is a number between 0 and 1 (0 means no bonds connected at the node are broken, and 1 means all the bonds are broken). Note that a damage index of around 0.4-0.5 indicates that a fracture surface exists if damage is localized along a surface (line). Diffuse damage regions may indicate a shattered zone or an area of densely packed cracks that are too fine to resolve with a certain discretization/horizon (see [20]). The legend shown in Figure 5 is used in all damage plots.

In Figure 5 to Figure **7**, the damage maps for the top face (x-y plane), bottom face (x-y plane), and cross-sectional cut (x-z plane) through the center of the glass plate are shown at about 77 μs. We compare our simulation results with experimental results for the three impact speeds, 61, 100, and 200 m/s.

4.2.1 Results for impact speed of 61 m/s

From Figure 5 we observe that radial cracks extend from the central crater region along the quadrant directions (towards the middle of the sides of the square plate) and the diagonal directions (towards the plate corners). For the region nearby the crater, radial cracks appear to be

straight (see damage on the bottom face in Figure 5(b)), and the diagonal cracks continue to be straight whereas the quadrant cracks have more turns. These features can also be distinguished in the experimental result in Figure 5(d). Circumferential or ripple cracks (see the highlighted elliptical areas) form in the computational model at about the same distance from the center as in the experiments. The mark left by the frame opening is much more prominent in the peridynamic simulations than in the experiment (see the highlighted rectangular areas) because in the computations we impose rigid, zero displacements conditions over where the metal frames are in the experimental setup. The damage maps also indicate another remarkable characteristic of fracture induced by impact on the G-PC system: in the diamond-shaped zones, a quadrant radial crack kinks just before reaching the boundary and the photograph of the experiment shows that the through-thickness crack is not perpendicular onto the plane of the plate, but it is rather tilted. A similar pattern is displayed by the peridynamic results, in which two quadrant cracks kink before reaching the boundary and the slight difference between the damage paths on the strike face and the back face of the glass plate means that these cracks are tilted through the thickness. Stress waves propagating through the G-PC system are responsible for these features.

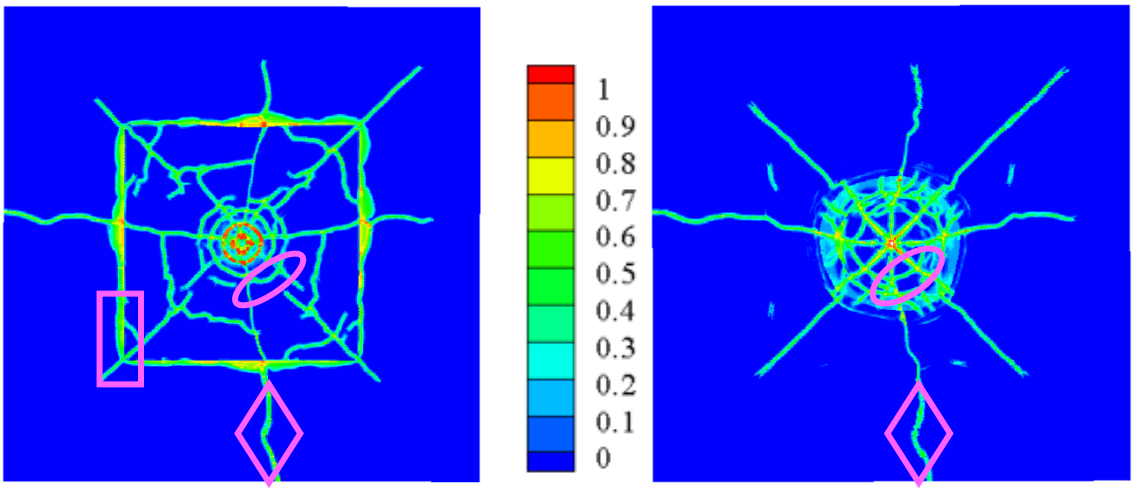

(a) (b)

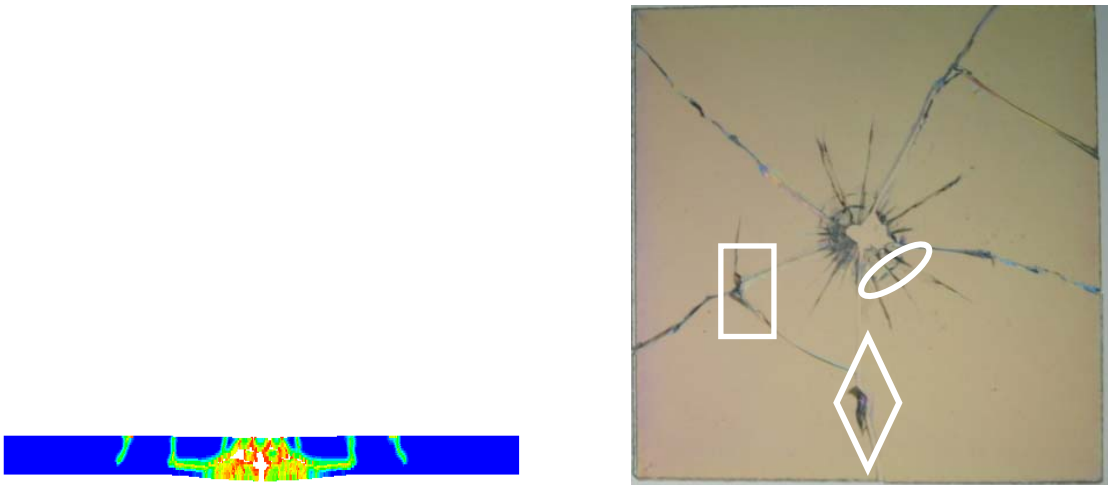

(c) (d)

Figure 5. Damage maps for impact speed of 61 m/s.The glass plate at about 77 μs: the strike face in (a), the bottom face in (b), and the central through-thickness cross section in (c), where displacements are enhanced by a factor of two, to better observe separation, and thickness direction is enlarged; experimental result shown in (d).

By examining the cross-sectional view of the peridynamics solution in Figure 5(c), we observe a Hertz-type cone crack combined with a spall-type fracture form in sequence as a result of the impact and wave reflections from the polycarbonate backing plate.

The time-evolution of the system of cracks for this impact velocity is discussed in Section 4.4.

4.2.2 Results for impact speed of 100 m/s

At the impact speed of 100m/s, the mark of the frame opening is now stronger, with cracks showing on both the strike and the back face of the glass plate (see Figure 6). As before, due to the more compliant response of the actual metal frame than the rigidly imposed boundary in our model, the experimental results indicate the presence of the frame opening in a much reduced way (see highlighted rectangular regions). Ripple cracks (marked by ellipses) now show farther away from the center of the plate than with the low impact speeds and they are not continuous but appear to be interrupted by radial cracks. The distinct difference between the damage on the strike face and back face of the glass plate near the center of the plate can be better understood from the cross-sectional view in Figure 6(c). It is interesting to remark that the blurry region, between the center of the plate and the first major ripple crack observed in the experimental results in Figure 6(d), is an indication of the conical crack we observed in the simulations (Figure

6(c)). The back face damage is extensive and diffuse damage (shattered glass) whereas on the front face, outside of the crater region, localized damage develops in the form of crack lines. Some cracks appear to start from the boundary of the structure in both the experiments and simulations (see zones marked by triangles). The quadrant cracks branch out (see regions marked by circles) as they approach the boundaries. In most cases, the corresponding crack paths on the strike face and back face of the glass plate are not identical, demonstrating that such cracks are slightly tilted in the thickness direction.

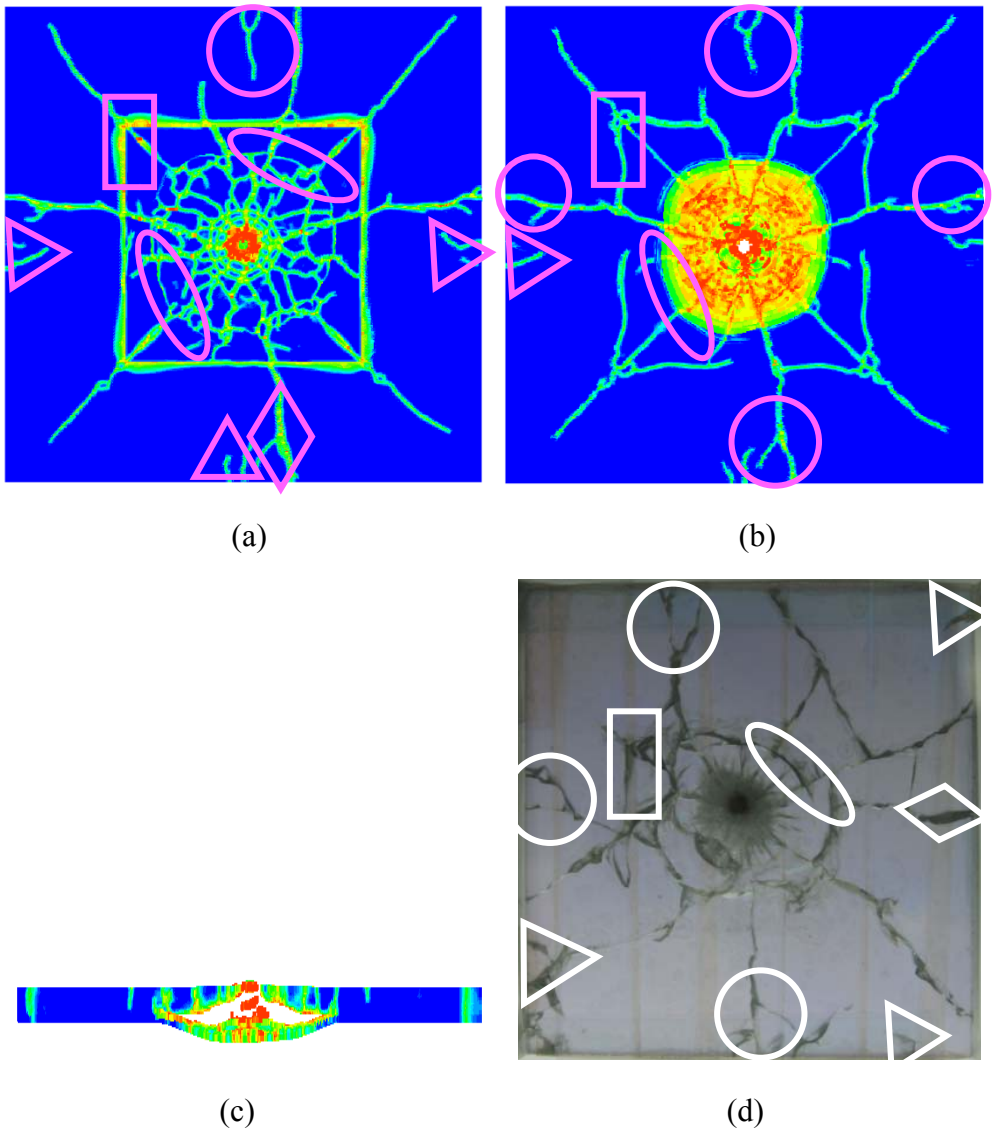

(a) (b)

(c) (d)

Figure 6. Damage maps for impact speed of 100 m/s. The glass plate at about 77 μs: the strike face in (a), the back face in (b), and the central through-thickness cross section in (c), where displacements are enhanced by a factor of two, to better observe separation, and thickness direction is enlarged; experimental result shown in (d).

This particular feature is seen in the photograph of the post-mortem sample as a darker and thicker crack line, due to the light reflection (see Figure 6(d)).

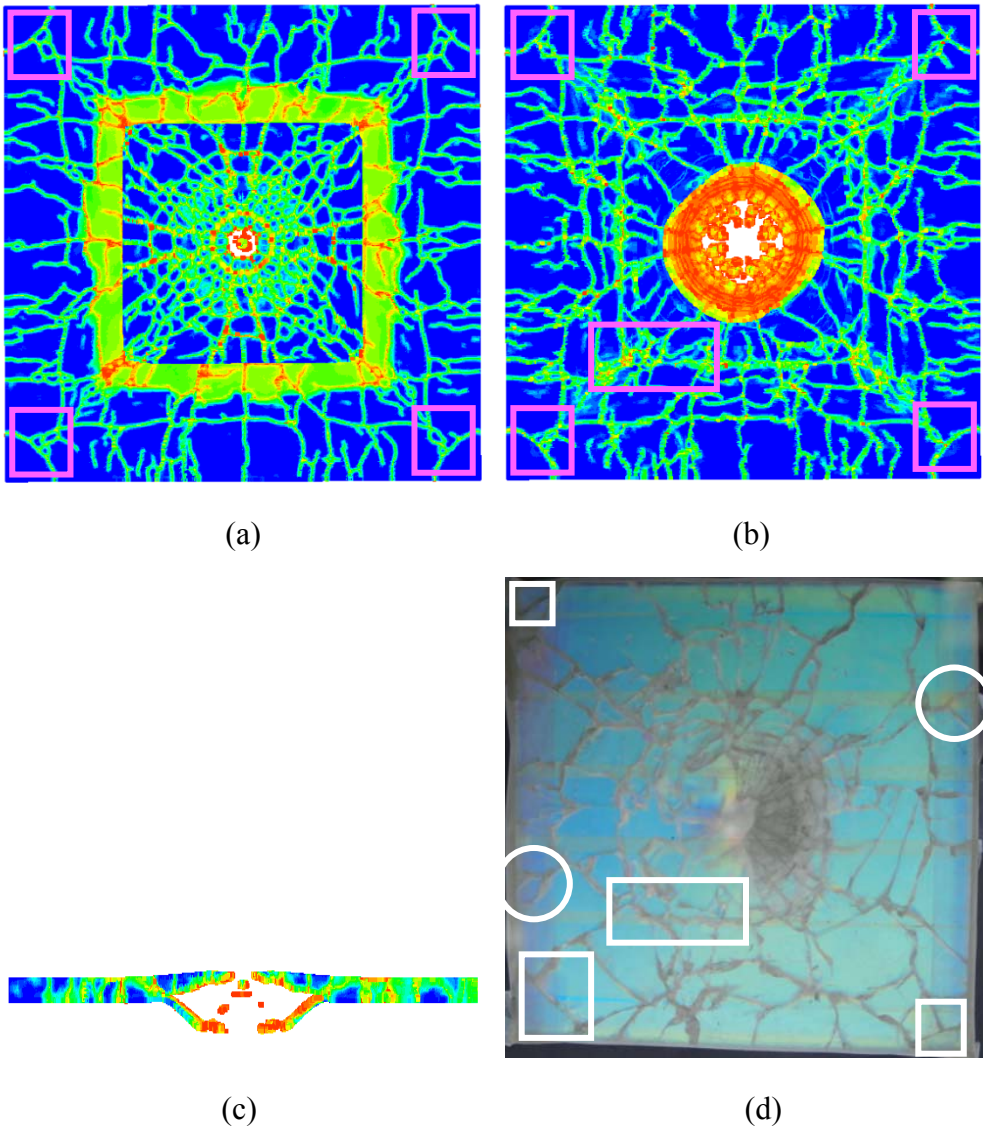

(a) (b)

(c) (d)

Figure 7. Damage maps for impact speed of 200 m/s. The glass plate at about 77 μs: the strike face in (a), the back face in (b), and the central through-thickness cross section in (c), where displacements are enhanced by a factor of two, to better observe separation, and thickness direction is enlarged; experimental result shown in (d).

4.2.3 Results for impact speed of 200 m/s

When the G-PC system is subject to impact speed of 200 m/s, the damage obtained by the peridynamic model is extensive and most of the glass layer is fragmented. Three different

regions can be identified from Figure 7 (a) and (b): a central region with finely spaced radial cracks on which a few ripple cracks superpose, a region that can be considered as the signature of the boundary conditions that mimic the frame opening, and the rest of the plate in which mostly large and some small size fragments are formed. These regions seen from the experiments are well captured by the peridynamic simulation, except for the signature cracks related to the frame opening: it is quite possible that under such impact energy, there is partial separation between the holding frame and the glass-polycarbonate plates and due to this, the frame opening signature is hardly visible (see the highlighted rectangular area in Figure 7(d)). In the simulations, considerable amount of damage is seen around the opening area and this is attributable to the rigid boundary conditions imposed there. The difference between the damage seen on the strike face and the back face in this respect is due to the presence of the backing polycarbonate plate that is in contact with the back face of the glass layer, whereas the top face of the glass layer has the imposed zero-displacements outside of the frame opening area. Since there is no energy dissipation mechanism in the model other than via breaking of bonds, stress waves create more damage than in the experiment where some of the energy is transferred to the metal frame and the holding fixture. Notice also that corner cracks (highlighted square regions) are a new feature seen in the experiments, not observed at the lower impact speed. The peridynamic simulations capture the corner cracks very well. For these corner cracks, the damage maps of the strike and back faces are similar, meaning that these cracks are straight through-thickness cracks, and not tilted. Some quadrant cracks still branch as they approach the boundaries (circular zones) and quite a few more cracks start from the boundaries and propagate inwards.

At this impact speed some plastic deformation is observed in the experiments in the polycarbonate layer, but no cracks. In the peridynamic solution, no damage forms in the polycarbonate layer. Since the peridynamic model used in this work does not include plastic deformation, and additional means to reduce the energy in the system, such as dissipation through the boundary conditions, are not present in our model, we observe a somewhat larger amount of glass layer damage from the computations, compared with the experimental results.

4.3 Trends with increasing projectile impact speed

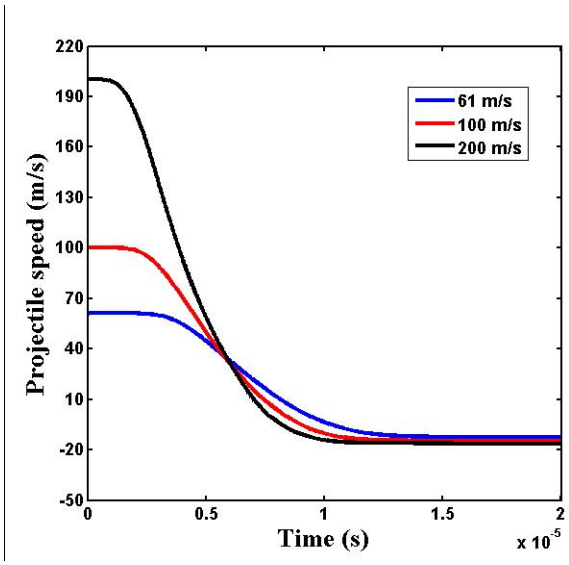

Figure 8. Evolution of the projectile speed at different impact velocities.

The projectile speed profiles are shown in Figure 8. Shortly after the projectile hits the target, it rebounds, thus the negative sign of the projectile speed, for all three cases tested. This coincides with the experimental observation. The magnitude of the rebound velocity, however, is slightly different from the experimental tests: at 61 m/s impact velocity the model gives a rebound speed of 13 m/s, while in the experiments it measures 3 m/s. At 100 m/s impact speed, the computations show a rebound speed of 15 m/s, while experimentally it measures about 8 m/s. For the 200 m/s case, the computations give 17 m/s while the measured value is 33 m/s. Notice also that the projectile time-in-contact with the target, estimated from the velocity plots in Figure 8 from the moment the speed starts to decrease until the moment the velocity becomes negative, is in the range of 6-7 μs. These contact times are significantly higher than when small projectiles (1 mm diameter) impact a glass block, measured to be between 1-2 μs (see [7]). The difference is due to the bending deformation of the G-PC system used in our work and the larger projectile size (5.56 mm diameter). In [7], the glass block is thick enough (2.5 cm) so that the stress waves generated at the time of impact did not return to the impact site after reflecting from the edges of the glass block, during the contact time. In our case (thickness of 0.33 cm), stress waves interact with the projectile.

While the trend observed in the experiments, of increased rebound velocity with an increasing impact speed, is matched by the peridynamic computations, two possible reasons are believed to contribute to the differences between the measured values and the peridynamic results:

- The use of a rigid model for the projectile: in reality the projectile deforms elasto-plastically and a complex transfer of energy between the deformable projectile and the PG-PC system takes place;
- Differences between the boundary conditions on the two-layer system that affect the bending structural response and thus the projectile rebound: in the experiments a metal frame and holding fixture are used, while in the simulations these conditions are replaced by imposed zero displacements.

Nevertheless, the fact that the trend of increasing rebound speed with an increased impact speed is well captured by this simple peridynamic model is encouraging.

4.4 The computed time-evolution of damage

In what follows we analyze the evolution of damage in the glass layer in the first 25 μs from impact. The 61 m/s impact speed is discussed here.

From the results shown in Figure 9 for the median cross-section through the thickness, we observe that the cracks start from the bottom face of the glass plate. These initial cracks are radial cracks in the form of an eight-spoke wheel. They propagate radially but also grow upwards through the thickness. This confirms the results from molecular dynamic simulations presented in [8]. The cracking from top to bottom has also been observed in computations of high velocity impact on a seven-layer glass system (see [22]). The first cracks on the top face form in the shape of a ring crack (see Figure 9 and Figure 10), around 5.2μs from the moment of impact.

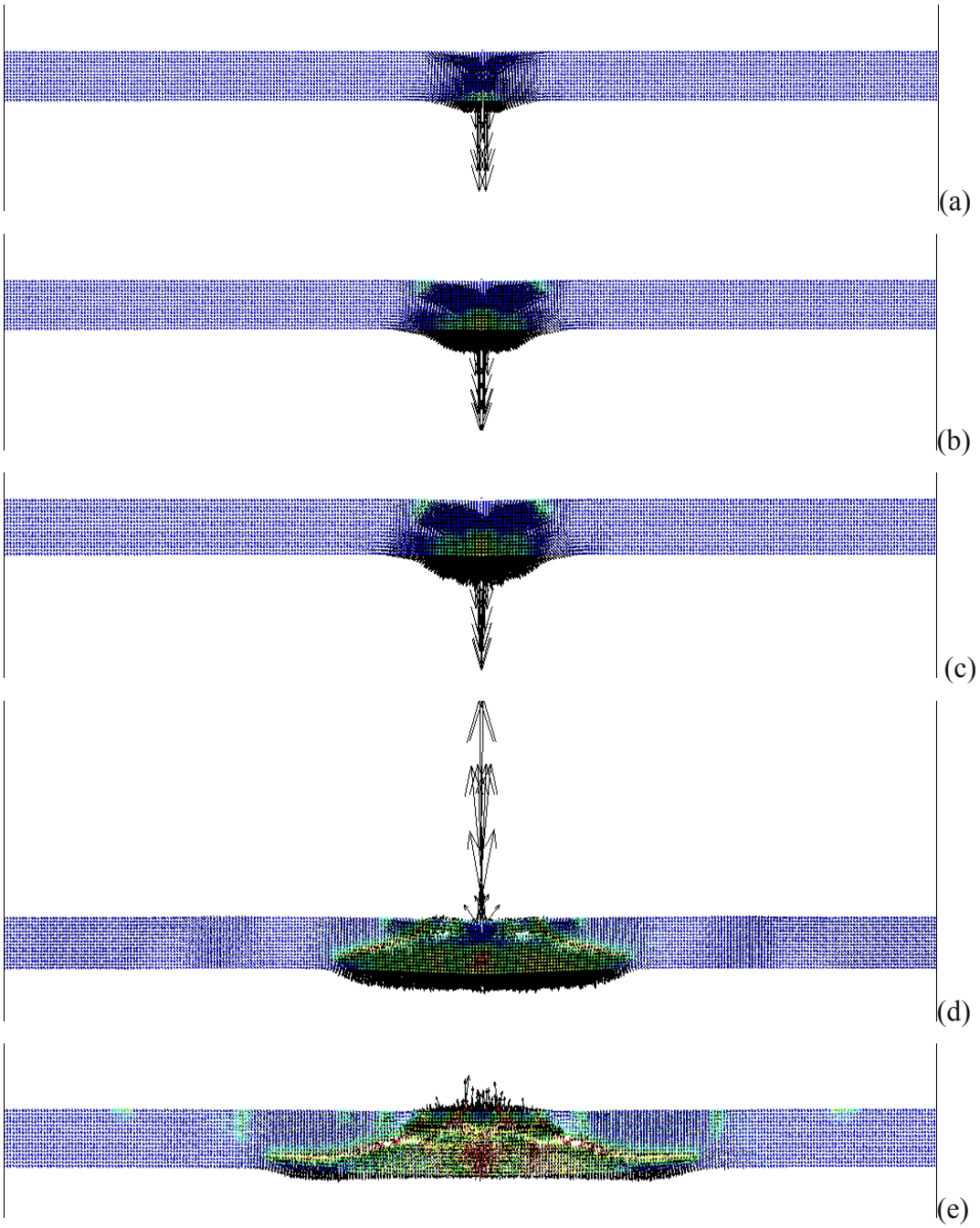

Figure 9. Evolution of damage and nodal velocities from the impact at 61 m/s. The central cross-section of the glass plate at 4.4, 5.2, 6, 11, and 25 μs (top to bottom). Nodal velocities are plotted using black arrows (quiver plot) on top of the damage maps.

Driven by the stress waves, the radial cracks from the bottom and the ring crack on the top face move towards one another and deflect from each other, before they coalesce. The crack interactions and the continuing propagation and reflection of stress waves in the system then lead

to the formation of other ring cracks on the top face, both inside and outside of the original ring crack of the top face. A Hertzian cone-crack is fully formed around 11 μs. The reflections from the boundaries (the frame region) further complicate the evolution of the damage, as can be seen from Figure 10. The presence of the boundary conditions that approximate the existence of the metal frame holding fixture generates straight cracks that propagate on the top face only. We call these "frame cracks". On the top face, wave interactions create conditions for glass chips to form in the middle of the inner bounds of the metal frame region. These surface cracks continue to grow as they propagate both towards the boundaries of the sample and along the frame cracks. Radial cracks grow and arrest before reaching the frame cracks, but eventually continue towards them, and cross them merging and getting ahead of the surface cracks. Radial cracks are primarily driven along the bottom face and they cut through to the top face as they propagate, but not always perpendicular to the faces.

The spokes in the 45-degree direction eventually arrest due to interactions with reflected waves, and only the so-called quadrant cracks (the horizontal and vertical spokes) continue to propagate, but their paths and speed of propagation are also perturbed by interactions with stress waves. Eventually, new diagonal cracks appear near the corners of the opening region and on the top face first, initiated by the interaction of waves that reflect from the sides of the frame opening. These cracks grow in both directions (towards the corners and the center) in the in-plane direction, and also grow through the thickness to give rise to diagonal cracks on the bottom face. At that stage, the diagonal cracks on the bottom face merge with the original diagonal cracks that started at the center.

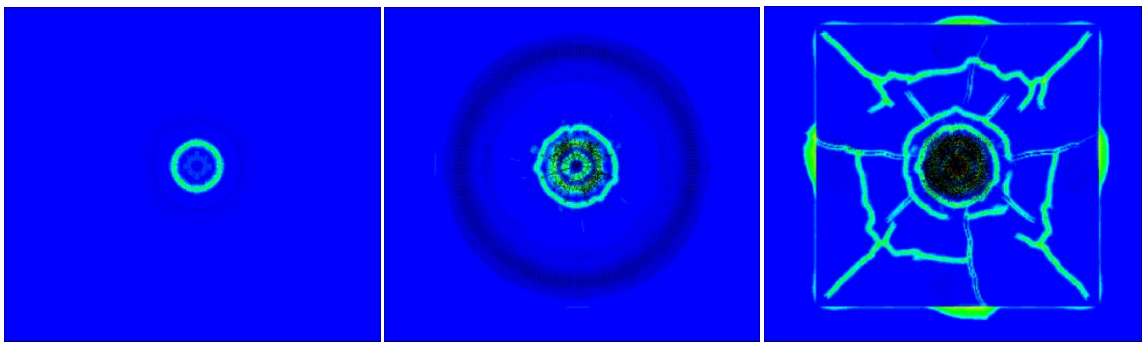

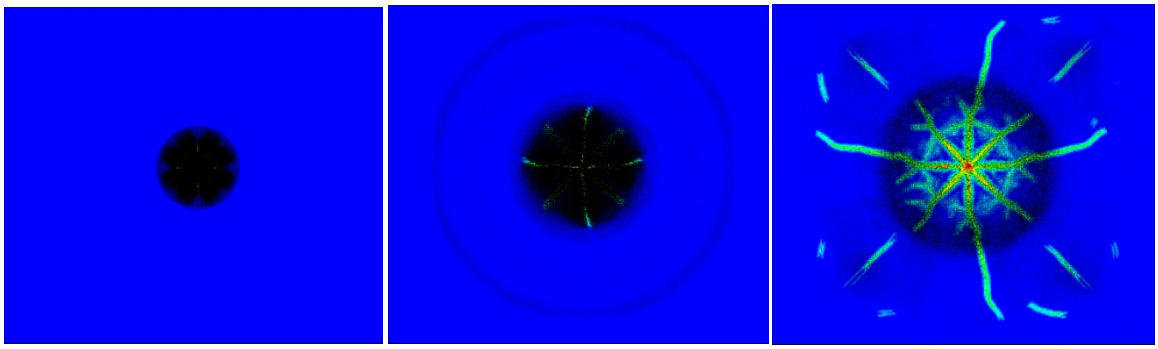

Figure 10. Evolution of damage and nodal velocities from the impact at 61 m/s. Top row: the top face of the glass plate at about 6, 11, and 25 μs (left to right). Bottom row: the bottom face of the glass plate at about 6, 11, and 25 μs. Nodal velocities are plotted using black arrows (quiver plot) on top of the damage maps.

The vector plots of the nodal velocity (see Figure 9 and Figure 10) superposed onto the damage index plots clearly indicate the propagation of the surface waves (Rayleigh waves) on the top and bottom faces of the glass plate. The complex interaction among longitudinal, shear, and surface waves, with the reflected waves from the boundaries and the polycarbonate interface, depict a complex picture of how damage is generated in the two-layer system at this impact velocity. Plans for the future include experimental setups capable of recording the evolution of damage in a two-layer system.

5. Conclusions

This paper presents experimental and numerical simulation results of the impact damage in a thin glass layer with polycarbonate backing subject to impact from a small spherical projectile at different speeds. Significant changes in the damage patterns that develop in the glass plate at three impact speeds take place in the experimental tests. These changes are predicted by the peridynamic model. Some very specific damage and crack features observed in experiments are, remarkably, reproduced by the computational model. The numerical results are obtained using the simplest peridynamic model for micro-elastic brittle materials. We can conclude that at these levels of loading, modeling the glass plate as a linear micro-elastic brittle material is sufficient to explain the damage structure from impact in the thin glass plate with a thin polycarbonate backing plate. The simplified boundary conditions used in the computational model is the most

important factor for the differences between the experiments and the computations in this problem.

In both the experiments and the peridynamic simulations, ejection of the projectile from the target is observed, and the trend of increasing rebound velocity with increased impact speed observed in experiments is reproduced by the peridynamic model. The computational results allow for an understanding of the complex evolution of damage in the glass layer induced by stress waves propagation and reflections
In the peridynamic model, no special crack initiation and propagation criteria and/or special meshing techniques are necessary.

Plans for the future include more accurate description of the holding fixtures/boundary conditions, which, in damage of brittle materials, are important factors that influence stress waves propagation in the system that control the evolution of failure fronts and the growth and propagation of damage in the system. Experimental setups capable of monitoring the time-evolution of damage are also planned.

Acknowledgement The authors are thankful for the financial support offered through research contracts between UNL and the ARO (Dr. Larry Russell), and ARL (project coordinators Dr. C.F. Yen and Dr. C. Randow), ARO award number 58450EG. The computations in this paper have been completed using facilities at the Holland Computing Center of the University of Nebraska-Lincoln.

References

[1] Knight CG , Swain MV , Chaudhri MM. Impacts of small steel spheres on glass surfaces. J Mater Sci 1977;12:1573-1586.

[2] Ball A , Mckenzie HW. On the low velocity impact behaviour of glass plates. J Phys IV 1994;4:783-788.

[3] Walley SM , Field JE. The contribution of the Cavendish Laboratory to the understanding of solid particle erosion mechanisms. Wear 2005;258:552-566.

[4] Field JE. Dynamic fracture: its study and application. Contemp. Phys. 1971;12:1-31.

[5] Field JE , "Investigation of the impact performance of various glass and ceramic systems.," European Research Office of the US Army, Report No. R&D 5087-MS-01, 1988.

[6] Field JE , Sun O. Townsend Ballistic impact of ceramics. Inst. Phys. Conf. Ser. 1989;102:387-393.

[7] Chaudhri MM , Walley SM. Damage to glass surfaces by the impact of small glass and steel spheres. Philos. Mag. A 1978;37:153-165.

[8] Bless SJ , Chen T. Impact damage in layered glass. Int J Fract 2010;162:151-158.

[9] Timmel M , Kolling S , Osterrieder P , DuBois PA. A finite element model for impact simulation with laminated glass. Int J Impact Eng 2007;34:1465-1478.

[10] Ismail J , Zairi F , Nait-Abdelaziz M , Azari Z. How cracks affect the contact characteristics during impact of solid particles on glass surface: A computational study using anisotropic continuum damage mechanics. Int J Impact Eng 2012;40-41:10-15.

[11] Pyttel T , Liebertz H , Cai J. Failure criterion for laminated glass under impact loading and its application in finite element simulation. Int J Impact Eng 2011;38:252-263.

[12] Holmstrom E , Samela J , Nordlund K. Atomistic simulations of fracture in sillica glass through hypervelocity impact. Europhys Lett 2011;96:16005-p1-16005-p5.

[13] Ravi-Chandar K , *Dynamic fracture*.: Elsevier, 2004.

[14] Silling SA , "Fragmentation modeling with EMU.," Sandia National Laboratories, Albuquerque, NM, Technical report 2005.

[15] Bobaru F , Ha YD. Adaptive refinement and multiscale modeling in 2D peridynamics. Int J Multiscale Comput Eng 2011;9:635-660.

[16] Silling SA. Reformulation of elasticity theory for discontinuities and long-range forces. J Mech Phys Solids 2000;48:175-209.

[17] Ha YD , Bobaru F. Studies of dynamic crack propagation and crack branching with peridynamics. Int J Fract 2010;162:229-244.

[18] Ha YD , Bobaru F. Characteristics of dynamic brittle fracture captured with peridynamics. Eng Fract Mech 2011;78:1156-1168.

[19] Hu W , Ha YD , Bobaru F. Modeling dynamic fracture and damage in fiber-reinforced composites

with peridynamics. Int J Multiscale Comput Eng 2011;9:707-726.

[20] Hu W , Ha YD , Bobaru F. Peridynamic simulations of dynamic fracture in unidirectional fiber-reinforced composites. Comput Meth Appl Mech Eng 2012;217-220:247-261.

[21] Bobaru F , Hu W. The meaning, selection, and use of the peridynamic horizon.. Int J Fract 2012;176:215-222.

[22] Bobaru F , YD Ha , W Hu. Damage progression from impact in multilayered glass modeled with peridynamics. Cen Eur J Eng 2012;[in print].

[23] Seleson P , Parks M. On the role of the influence function in the peridynamic theory. Int J Multiscale Comput Eng 2011;9:689-706.

[24] Weckner O , Silling SA. Determination of nonlocal constitutive equations from phonon dispersion relations. Int J Multiscale Comput Eng 2011;9:623-634.

[25] Silling SA , Askari E. A meshfree method based on peridynamic model of solid mechanics. Comput Struct 2005;83:1526-1535.

[26] Silling SA , Epton M , Weckner O , Xu J , Askari E. Peridynamic states and constitutive modeling. Journal of Elasticity 2007;88:151-184.

[27] Hu W , "Peridynamic models for dynamic brittle fracture," University of Nebraksa-Lincoln, Lincoln, NE, Ph.D. dissertation. 2012.